

Article

Enhancing a Deep Learning Model for the Steam Reforming Process Using Data Augmentation Techniques

Zofia Pizoń ¹, Shinji Kimijima ² and Grzegorz Brus ^{2,*}

¹ Department of Fundamental Research in Energy Engineering, Faculty of Energy and Fuel, AGH University of Krakow, 30059 Mickiewicza Ave., 30-059 Krakow, Poland

² Department of Machinery and Control Systems, Faculty of Mechanical Engineering, Shibaura Institute of Technology, Tokyo 135-8548, Japan; kimi@sic.shibaura-it.ac.jp

* Correspondence: brus@agh.edu.pl

Abstract: Methane steam reforming is the foremost method for hydrogen production, and it has been studied through experiments and diverse computational models to enhance its energy efficiency. This study focuses on employing an artificial neural network as a model of the methane steam reforming process. The proposed data-driven model predicts the output mixture's composition based on reactor operating conditions, such as the temperature, steam-to-methane ratio, nitrogen-to-methane ratio, methane flow, and nickel catalyst mass. The network, a feedforward type, underwent training with a comprehensive dataset augmentation strategy that augments the primary experimental dataset through interpolation and theoretical simulations of the process, ensuring a robust model training phase. Additionally, it introduces weights to evaluate the relative significance of different data categories (experimental, interpolated, and theoretical) within the dataset. The optimal artificial neural network architecture was determined by evaluating various configurations, with the aim of minimizing the mean squared error (0.00022) and maximizing the Pearson correlation coefficient (0.97) and Spearman correlation coefficient (1.00).

Keywords: methane steam reforming; hydrogen; deep learning; reaction kinetics



Citation: Pizoń, Z.; Kimijima, S.; Brus, G. Enhancing a Deep Learning Model for the Steam Reforming Process Using Data Augmentation Techniques. *Energies* **2024**, *17*, 2413. <https://doi.org/10.3390/en17102413>

Academic Editors: Matteo Genovese, Francesco Piraino and Petronilla Fragiacomio

Received: 5 April 2024
Revised: 10 May 2024
Accepted: 14 May 2024
Published: 17 May 2024



Copyright: © 2024 by the authors. Licensee MDPI, Basel, Switzerland. This article is an open access article distributed under the terms and conditions of the Creative Commons Attribution (CC BY) license (<https://creativecommons.org/licenses/by/4.0/>).

1. Introduction

Hydrogen represents a promising alternative energy carrier. It can be produced from renewable or non-renewable energy sources [1]. Despite the newest reports indicating possible accumulations of hydrogen in geological formations [2,3], by 2023, 84% of the hydrogen produced came from fossil sources, including 62% from natural gas, according to data from the International Energy Agency (IEA) [4]. The steam reforming of methane is recognized as the predominant technique for hydrogen production. It represents the oldest and most extensively documented method of generation of H₂. The process does not require an oxygen supply. It is conducted at temperatures lower than those of alternative methods. Furthermore, the hydrogen-to-carbon monoxide ratio in the post-reaction mixture always exceeds unity. However, this process is associated with the emission of the highest amounts of greenhouse gases into the atmosphere [5]. Steam reforming is an endothermic process, which means that it requires heat and is typically facilitated by catalysts, often nickel-based [6]. The process is carried out with an excess of steam to prevent the deposition of soot on the catalyst and reactor walls [7]. The following chemical equations for methane steam reforming (MSR) and the Water–Gas Shift Reaction (WGSR) capture the core of the process:



The steam reforming of hydrocarbons was used to produce synthetic gas in the early twentieth century [7]. The hydrogen produced was used in the synthesis of ammonia and methanol and also in the petroleum industry for hydrotreating and hydro-cracking [8]. Currently, hydrogen produced by steam reforming is increasingly used as an energy carrier. The chemical energy stored in hydrogen can be transformed into electricity through the use of fuel cells. The use of hydrogen in this manner requires the miniaturization of reforming reactors compared to their industrial counterparts [9]. Consequently, there is a significant demand for process optimization, for which computer simulations are necessary [10]. Scientists employ various methodologies to investigate the subject. For instance, they develop kinetic models based on the Arrhenius equation and reaction rate equation [11] to accurately predict the composition of post-reaction mixtures. L. van Biert et al. [12] utilized the Langmuir–Hinshelwood mechanism to simulate changes in temperature profiles and reactant concentrations during the direct steam reforming of methane within solid oxide fuel cells. In addition, computational fluid dynamics (CFD) is employed to simulate methane steam reforming. K. Chen et al. [13] developed a parallel kinetic model of the reaction in which methane and steam react simultaneously to produce carbon monoxide and carbon dioxide. Subsequently, they conducted a sensitivity analysis of the steam-to-methane (SC) ratio, inlet gas flow rate, and temperature. D. Pashchenko et al. [14] developed a new method based on the Fourier–Kirchoff thermal conductivity equation. Utilizing the CFD model, the temperature distribution inside the catalyst particle was determined. It was found to be irregular, and the maximum temperature value did not occur at the center of the particles. A. Amini et al. [15] developed a CFD simulation of an industrial reformer tube. Through sensitivity analysis, they investigated the influence of reformer operating parameters on hydrogen production. Additionally, the optimal conditions were determined with the reformer tube length set at 11 m, tube diameter at 0.172 m, SC at 1.6, feed flow rate at 0.34 kg s^{-1} , and surface heat flux at 95 kW m^{-2} .

The integration of artificial intelligence algorithms further enhances the efficiency of this optimization process. N. Dat Vo et al. [16] generated and validated a mathematical model of a methane steam reforming reactor. Then, the model was used to generate a dataset on the impact of the operating parameters (the inlet flow rate, the steam-to-carbon ratio of the reactor side, temperature, and the inlet flow rate of the furnace side) on the reactor's performance. The dataset was used to train a feedforward-backpropagation artificial neural network (ANN) to map the relationship between the operating parameters and the predicted outputs. The results generated with the ANN were characterized by high accuracy (98.91%) and a short computational time of 2 s. Ayodele et al. [17] used a multilayer perceptron–artificial neural network (MLP-ANN) and a nonlinear response surface method to predict the hydrogen concentration in the post-reforming mixture based on the values of temperature, methane, and steam partial pressures. The network was trained using experimental measurements. The MLP-ANN model obtained better prediction results than the nonlinear response surface method, with R^2 equal to 0.988. In the article by Nkulikiyinka et al. [18], ANN and random forest models were used as soft sensor models to predict gas concentrations in reformer and regenerator reactors in the process of sorption-enhanced steam methane reforming. The prediction was based on the following operating parameters: pressure, temperature, steam-to-carbon ratio, and sorbent-to-carbon ratio. Both models were characterized by an R^2 value higher than 0.98, but the random forest model was more accurate with a lower mean absolute error value (0.002–0.014) than the ANN model (0.005–0.024). Z. Liu et al. [19] proposed a universal microkinetic–machine learning method to screen bimetallic catalysts. First, a microkinetic model was designed to search for descriptors and activity ranges. Then, four machine learning models were built to predict the formation energies of key descriptors. The obtained results were used as input data to optimize the microkinetic model. Finally, bimetallic catalysts from the database were compared in terms of activity, stability, and cost. The authors selected the best learning model, which was XGBoost, with an R^2 coefficient value of 0.973. Of the eight metallic catalysts, Rh, Ni, and Ir exhibited

high activity, which is consistent with the experimental results. Furthermore, the designed model identified 48 active, stable, and cost-effective methane-reforming catalysts. Y. Wang et al. [20] conducted the performance optimization of a solid oxide fuel cell (SOFC) in which direct internal steam reforming takes place. Initially, they created a cell model, which they used to generate a dataset to train an artificial neural network. The network was able to describe the relationships between the cell operating conditions and its performance parameters. Subsequently, the ANN was integrated with a sensitivity analysis algorithm to determine the importance of the cell operating conditions and optimize them. The applied algorithm enables a significant reduction in the carbon deposition rate while maintaining a high power density and a safe temperature gradient (below 10 K cm^{-1}). An artificial network was also used to optimize integrated sorption-enhanced steam methane reforming (SESMR) [21]. After conducting a sensitivity analysis of the system, it was concluded that the pressure swing adsorption variables distinctly affected product quality, while the cyclic fluidized bed variables mainly contributed to other performance parameters. The ANN-based optimization model was integrated with the economic model. Under optimal conditions, the cost of 99.99% purity hydrogen production using the SESMR process is equal to $1.7 \text{ USD} \cdot \text{kg}^{-1}$. The cost is 15% lower compared to the process without carbon dioxide capture. The ANN can also be used to optimize the steam-to-biogas ratio in a biogas-fueled solid oxide fuel cell [22]. The authors of the article studied the correlation between the steam-to-biogas ratio as a function of the operating temperature and biogas composition. They found that for the temperature range of 873 K–1273 K and the biogas methane-to-carbon dioxide ratio range of 0.82–3, the optimal steam-to-biogas ratio is equal to 0.3–1.3. Hossain et al. [23] compared two artificial neural network models, one based on a multilayer perceptron (MLP) and the other based on a Radial Basis Function (RBF). They found that the MLP performed better than the RBF in predicting syngas composition resulting from reforming over Ni/CaFe₂O₄ catalysts. The MLP-based model showed a higher coefficient of determination (R^2) values for the prediction of H₂ yield, CO yield, CH₄ conversion, and CO₂ conversion. Statistical analysis further confirmed the significance of the MLP-based model, demonstrating superior predictive capability. Deng and Guo [24] used an artificial neural network to predict the products of methane reforming using CO₂ and steam under varying conditions. The study demonstrated that the best-performing network was capable of making reliable predictions even when operating conditions were beyond the training ranges. This study shows how artificial intelligence can be used to optimize the methane bi-reforming process for syngas production with a flexible H₂/CO ratio, contributing to the efficient utilization of methane-rich gases. Pajak et al. [25–27] used a genetic algorithm to propose an optimal catalyst distribution in a small-scale methane steam reformer. Their algorithm screened hundreds of solutions to select those that best fit the maximum conversion rate and uniform temperature distribution criteria. The fitness function consists of a two-dimensional computational fluid dynamics model of a small-scale reformer, which could benefit from faster machine learning solutions such as deep learning in place of classical numerical simulation.

Morlanes et al. [28] developed a methodology that uses artificial neural networks to fit a kinetic model for the steam reforming of hexane and heptane with a NiMgAl catalyst. The versatility and strength of this data-driven approach were demonstrated by validating the models under a wide range of experimental conditions and with different feeds. This methodology offers a promising alternative for the kinetic modeling of steam reforming processes. In a recent review of artificial neural networks applied to model hydrogen production by Bilgic et al. [29], the authors demonstrated improvements in the modeling accuracy and overall results when hybrid models incorporating ANNs are used. The review highlights the critical role of ANNs in simulating hydrogen production due to their nonlinear programmability and suggests that experimenting with new ANN combinations could further enhance prediction performance. The conclusion emphasizes that ANNs offer a cost-effective strategy for optimizing and controlling hydrogen production processes. It

also stresses the urgent need for further research and experimental data to improve ANN models, invoking a sense of importance and urgency in contributing to this field.

As evidenced in the literature review, accurate neural network simulations of the reforming process play an increasing role in predicting reactor performance and optimizing operational parameters, thus enhancing efficiency and reducing costs. The reliability of these simulations ensures the development of effective energy production strategies, particularly in hydrogen generation through steam reforming. This study contributes to these efforts by proposing a neural network simulation of the reforming process that can correctly reproduce the empirical data using a combination of numerical simulation and empirical datasets. Unlike previous simulations, our approach utilizes a genetic algorithm to fine-tune the empirical parameters within the reaction kinetic model, ensuring the best fit with experimental observations. This article is organized as follows: The Introduction presented above (Section 1) sets the context for the research, focusing on the methane steam reforming process as a widespread method for hydrogen production; it presents machine learning techniques, particularly deep learning, which can improve reaction kinetic simulations and thereby contribute to new reactor designs. Research Methodology, presented in the next section (Section 2), discusses the methodology and development of the proposed artificial neural network model. This includes the design of the ANN to predict the composition of the post-reaction mixture based on variable reactor operating parameters and the use of data augmentation techniques involving experimental, interpolated, and theoretical data. Section 3, Results, presents the outcomes of the ANN predictions, comparing them with experimental data and test data. It discusses the dependencies of the molar fractions of components at the reactor outlet on the steam-to-methane ratio and the effect of the reaction temperature on the post-reaction mixture composition. The conclusion, Section 4, summarizes the findings, emphasizing the ANN's ability to predict the post-reaction mixture composition based on reactor operating parameters. It also mentions the selection of the optimal network structure based on statistical analysis and suggests areas for future model improvement.

2. Research Methodology

In this study, the methane steam reforming process is modeled using an artificial neural network. The effectiveness of this model depends on the architecture and efficiency of the training method, which is a process of adjusting the weights and biases of the network to best represent the provided training data. A model with insufficient layers and neurons may struggle with the training process. Moreover, an oversimplified model might lead to methodological errors and a prediction that does not align well with the problem it aims to solve. However, a model that is too large can slow the optimization process and prolong the training duration. In addition, a model that is too large can lead to overfitting, where it becomes overly tailored to the training data, rendering it ineffective for tasks outside the training. Therefore, it is crucial to select a network architecture that fits the specific issue of methane steam reforming.

The presented work focuses on numerical experiments to choose a suitable network architecture to simulate the methane steam reforming process, which requires a complex model to process input data on the catalyst load and operational conditions without overfitting the training data. The first stage of the work was to prepare a set of training data. The set consisted of three types of training data: experimental [30], interpolated, and theoretical [30] data.

2.1. Experimental Dataset

The present studies reused experimental data from our previous studies published elsewhere [30]. The following is a brief description of the experiment used to obtain the experimental dataset. The experimental framework is shown in Figure 1. A stainless steel reformer was located within an electric furnace and capable of reaching temperatures up to 1000 °C. The preheater and afterheater within this system have a maximum operating

temperature of 400 °C, although for the purposes of our experiments, they were kept consistently at 200 °C. The thermal conditions were monitored with four thermocouples placed as depicted in Figure 1 (indicated as “T”). A thin layer of catalyst was as shown in Figure 1 and covered with alumina balls, which were used for preheating. High-purity methane served as fuel and was channeled to the reformer through a flow controller, marked “F” in Figure 1, and an evaporator that also functioned as a preheater and a static mixer. Water was introduced into the system through a pump and fed to the evaporator. After reformation, the gas composition was examined using gas chromatography after condensing the steam by cooling the gas mixture to 2 °C. The reformer reaction tube was packed with a nickel catalyst supported on yttria-stabilized zirconia, a commercial catalyst supplied by AGC SEIMI CHEMICAL CO [31]. This catalyst, in fine powder form, consisted of 60% vol NiO and 60% vol YSZ, aligned with the typical nickel-to-YSZ ratio of 40–60%. The catalyst particles were spherical, with a diameter of 0.85 μm and a specific surface area of 5.2 m² g⁻¹ [31]. Before the introduction of methane, the catalyst was kept at 800 °C for 6 h in a mixture of nitrogen (150 mL min⁻¹) and hydrogen (100 mL min⁻¹) to facilitate the reduction of NiO to Ni. The reaction tube was modified, including partial filling with Al₂O₃, to counteract the cooling effect of the inflow. The gas mixture was preheated to the reaction temperature by the electric furnace before entering the reaction zone. Ensuring that the reaction permeated the entire catalyst volume, which is crucial for accurate kinetic data, necessitated maintaining a low methane conversion rate, achieved by diluting the methane with nitrogen. Nitrogen, although not a reactant, alters partial pressures, thus reducing the reaction rate and methane conversion. All experimental data were recorded under atmospheric conditions, and the geometric specifications of the reactor are detailed in Table 1.

Table 1. Reactor properties [30] (with permission from Elsevier).

Type	Bed Height	Radius	Length
Stainless steel	1.0 mm	25.4 mm	450 mm

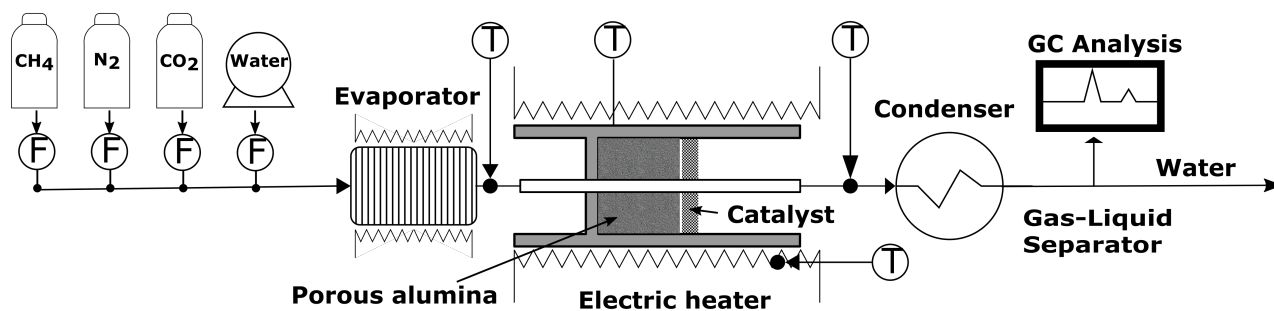


Figure 1. A schematic view of the experimental setup.

The experimental data that describe the relationship between the post-reaction mixture composition and the temperature were interpolated. Spline interpolation with not-a-knot end conditions was utilized. This method involves interpolating the value at a query point based on cubic interpolation using the values at neighboring grid points.

2.2. Mathematical Model

The model was based on the following reaction rate equation [30]:

$$r_{st} = w'_{cat} \cdot A \cdot \exp\left\{\left(-\frac{E}{RT}\right)\right\} \cdot p_{CH_4}^a \cdot p_{H_2O}^b \quad (3)$$

where r_{st} —reaction rate in mol s⁻¹ m⁻³; w'_{cat} —catalyst density in g m⁻³; $A = 2.582 \cdot 10^{-4}$ mol g⁻¹ Pa^{-(a+b)} s⁻¹—pre-exponential constant; $E = 115,255$ J mol⁻¹—

activation energy; $R = 8.314472 \text{ J mol}^{-1} \text{ K}^{-1}$ —universal gas constant; T —temperature of reaction in K; p_{CH_4} —partial pressure of methane in Pa; $p_{\text{H}_2\text{O}}$ —partial pressure of steam in Pa; and $a = 1.0$, $b = 0.0$ —dimensionless coefficients corresponding to the reaction order. The values of the rate equation coefficients (A, E, a, b) were determined using a genetic algorithm by fitting them to experimental data. The system of equations to be solved was based on the methane steam reforming reaction conversion rate and equilibrium equation for the shift reaction. The obtained set of two equations is presented below:

$$\begin{cases} x_{\text{st}} = 1 - (\dot{n}_{\text{CH}_4}^{\text{inlet}} - r_{\text{st}}) / \dot{n}_{\text{CH}_4}^{\text{inlet}} \\ y(3x_{\text{st}} + x_{\text{sh}}) - K_{\text{sh}}(x_{\text{st}} - x_{\text{sh}})(SC - x_{\text{st}} - x_{\text{sh}}) = 0 \end{cases} \quad (4)$$

where

$$K_{\text{sh}} = \exp\left(-\frac{\Delta G_{\text{sh}}^0}{RT}\right) \quad (5)$$

where G_{sh} is the change in standard Gibbs free energy of the shift reaction. The equilibrium constant given by Equation (5) is introduced into Equation (4) to calculate the conversion rate of the shift reaction. The mass production or consumption rate of each chemical species by the fuel reforming reaction (Equation (1)) and shift reaction (Equation (2)) was calculated from reaction stoichiometry, as indicated in Table 2.

Table 2. Changes in chemical components inside the fuel reformer [30] (with permission from Elsevier).

Gas	Inlet ¹	Steam Ref.	Shift	Outlet
CH ₄	1	x_{st}	0	$1 - x_{\text{st}}$
H ₂ O	SC	$-x_{\text{st}}$	$-x_{\text{sh}}$	$SC - x_{\text{st}} - x_{\text{sh}}$
H ₂	0	$-3x_{\text{st}}$	x_{sh}	$3x_{\text{st}} + x_{\text{sh}}$
CO	0	x_{st}	$-x_{\text{sh}}$	$x_{\text{st}} - x_{\text{sh}}$
CO ₂	CC	0	x_{sh}	$CC + x_{\text{sh}}$

¹ For 1 mol of methane.

The mathematical model was used because of the good agreement between the simulation and experimental results (mean Pearson correlation equal to 0.997). Additionally, it depicts the course of the process under kinetic conditions consistent with experimental conditions.

2.3. Accounting for Dataset Significance

The dataset contained information about the influence of five variable operating parameters (temperature, steam-to-methane ratio (SC), nitrogen-to-methane ratio (NC), nickel catalyst mass, and inlet methane flow rate) on the concentration of post-reaction mixture components: hydrogen, methane, carbon monoxide, and carbon dioxide. Data were collected and weighted for significance, prioritizing experimental data to enhance their importance. Originally, the experimental dataset contained 72 records; this number expanded to 729 after applying duplication to emphasize their significance. Initially, the interpolated dataset held 238 records, which later increased to 305 through augmentation. The theoretical data generated encompassed 9441 records. Due to the limited amount of experimental data, a large amount of theoretical data had to be utilized. The weights of the data were selected by trial and error. The data augmentation method is presented in Figure 2. Subsequently, the data were scaled to the range [0, 1] to facilitate the ANN training process.

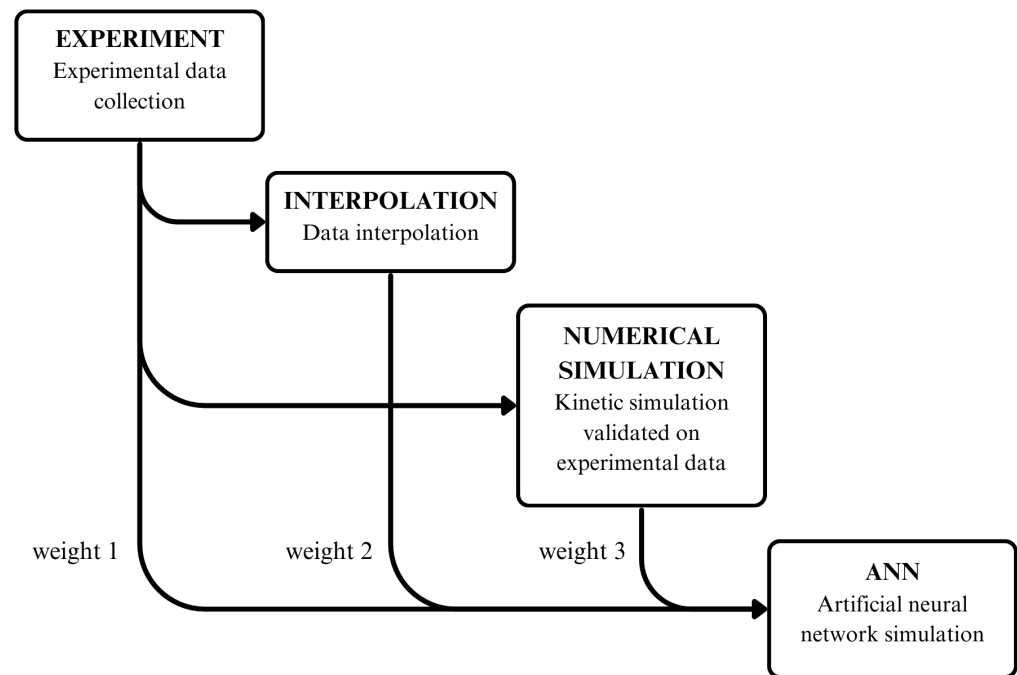


Figure 2. Used data augmentation method.

2.4. Selecting Network Architecture

Various network architectures were examined and compared using statistical analysis. The log-sigmoid transfer function for neuron activation was employed in the first hidden layers, and the softmax transfer function was employed in the last hidden layer. The chosen activation functions are designed to keep values within the interval $[0, 1]$. Additionally, by using the softmax function, the output values are transformed into a probability distribution, improving the model's physicality. The Broyden, Fletcher, Goldfarb, and Shanno (BFGS) Quasi-Newton Backpropagation algorithm was selected for the training method. The MATLAB Software R2023b with Deep Learning toolbox was used.

The mean squared error (MSE) values were compared to select the best network architecture. Mean squared error is a performance function calculated using the following formula:

$$MSE = \frac{\sum_{i=1}^n (x_i - y_i)^2}{n}, \quad (6)$$

where x_i —real value; y_i —predicted value; and n —number of values. The details of the conducted numerical experiment are presented in Table A1 in the Appendix A. The lowest error value achieved was 0.00020 for the network labeled as number twenty-three. This network consisted of an input layer, an output layer, and seven hidden layers. The consecutive hidden layers consisted of twelve, fourteen, sixteen, fourteen, twelve, ten, and eight neurons. The training process lasted for 4000 epochs. For five networks whose simulations achieved the lowest values of mean squared error, i.e., labeled as numbers eleven, seventeen, twenty, twenty-three, and twenty-four, Pearson correlation coefficients and Spearman correlation coefficients between the simulation results and the values of the test data were calculated. The Pearson correlation coefficient is defined by the following formula:

$$r_P = \frac{\sum_{i=1}^n ((x_i - \bar{x})(y_i - \bar{y}))}{(n-1) S_x S_y}, \quad (7)$$

x_i —test value; \bar{x} —mean test value; y_i —predicted value; \bar{y} —mean predicted value; n —number of values; and S_x and S_y —standard deviations calculated from test values and predicted values. The formula for the Spearman correlation coefficient is as follows:

$$r_s = \frac{1 - 6 \sum_{i=1}^n (y_i - \bar{y})^2}{n(n^2 - 1)}, \quad (8)$$

where y_i —predicted value; \bar{y} —mean predicted value; and n —number of values. Calculations were performed for each test component of the post-reaction mixture. Subsequently, the mean values of both coefficients were calculated for each network. The results of the calculations are presented in Table 3. For all five selected network architecture variants, the mean Pearson correlation coefficients and Spearman correlation coefficients achieved high values. The highest mean values of the Spearman correlation coefficient were obtained for the networks labeled as numbers eleven, seventeen, twenty-three, and twenty-four. The highest mean Pearson correlation coefficient, equal to 0.965, was obtained for the network labeled as number eleven. This network consisted of an input layer, an output layer, and three hidden layers. The hidden layers comprised six, eight, and six neurons, and the training process lasted for 6000 epochs. The selected model was notable for its versatility and broader applicability. This allows the model to enhance its robustness during training and effectively address training data loss errors.

Table 3. Values of mean Pearson correlation coefficients and mean Spearman correlation coefficients for subsequent variants of network architectures.

No.	Number of Hidden Layers	Vector of the Number of Neurons in Hidden Layers	Number of Epochs	Mean Pearson Correlation Coefficient	Mean Spearman Correlation Coefficient
11	3	[6 8 6]	6000	0.965	1.000
17	5	[6 8 10 8 6]	40,000	0.953	1.000
20	5	[8 10 12 10 8]	25,000	0.964	0.991
23	7	[12 14 16 14 12 10 8]	4000	0.953	1.000
24	7	[12 14 16 14 12 10 8]	36,000	0.955	1.000

Figure 3 shows the change in the mean squared error during the training process of the chosen ANN architecture (labeled as number eleven). As the model undergoes training epochs, there is a noticeable downward trend in the MSE values, indicating an improvement in the model's ability to fit the data. The absence of overfitting can be observed because the error values do not increase. The lowest value of mean squared error was marked in the green circle. This suggests that the model is effectively learning from the training data and generalizing well to unseen validation and test data, which is a positive indication of its performance.

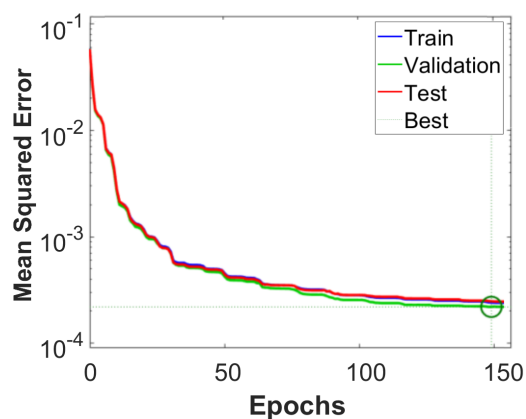


Figure 3. The dependence of the mean squared error on the number of epochs in the training process.

Accurate neural network simulations of the reforming process play a crucial role in forecasting reactor performance and fine-tuning operational parameters. Therefore, a falsification endeavor, which involves comparing experimental data with numerical predictions, will be elaborated on in the following section.

3. Results

The concentrations of individual components of the post-reaction mixture were calculated to investigate the response of the reforming reaction progress with the change in various reactor operating parameters. The simulations were conducted using the network labeled as number eleven, and the test data were compared to evaluate the accuracy of the prediction of the ANN. From various conducted simulations, four cases were selected to present in this paper.

To investigate the response of the post-reaction mixture to the methane flow rate, the molar fraction of each gas component was calculated at the outlet of the reactor. Figure 4 shows the results of the ANN simulation, presented as continuous lines, versus the test kinetic simulation data, shown as dotted lines. As can be seen in the figure, the artificial neural network could closely reproduce the validation results. Here, we found that the methane flow rate increases, the concentration of unreacted methane increases, and the concentrations of reforming products decrease, which is a natural consequence of the limited reaction rate. This suggests that the network can be used to predict the post-reaction mixture in the verified flow rate ranges.

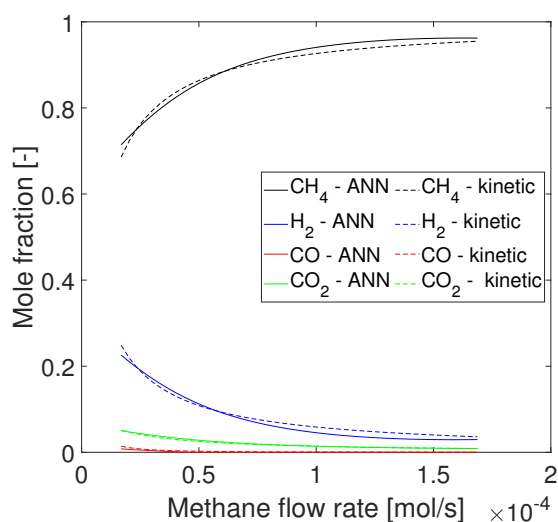


Figure 4. Comparison of ANN simulation results with test data (kinetic simulation data) for variable methane flow rate values and $T = 625$ °C; $NC = 3.00$; $SC = 3.00$; $m_{Ni} = 1.48$ g.

Figure 5 shows the concentrations of components in the post-reaction mixture as a function of the nickel catalyst mass. Kinetic simulation results are presented as dotted lines, whereas continuous lines represent ANN predictions. As the catalyst mass increases, hydrogen, carbon monoxide, and carbon dioxide concentrations increase, and the methane concentration decreases. Again, such a response of the system is consistent with the existing knowledge of the process chemistry, as all measurements were taken in the kinetic regime of the reaction [30]. It is important to note that all training data were obtained for the reaction in a kinetic regime, far from equilibrium; if the amount of catalyst further increases and the reaction approaches equilibrium, the prediction of the network might differ from the experiment since it was trained only in the kinetic regime.

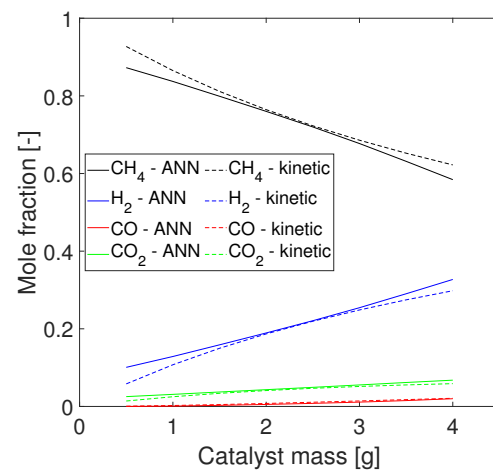


Figure 5. Comparison of ANN simulation results with test data (kinetic simulation data) for variable catalyst mass values and $T = 625\text{ °C}$; $NC = 3.00$; $SC = 3.00$; $f_{CH_4} = 3.38 \cdot 10^{-5}\text{ mol s}^{-1}$.

Figure 6 shows the dependencies of the molar fractions of components at the reactor outlet on the steam-to-methane ratio. Dotted lines illustrate the test data, while the ANN predictions are depicted by continuous lines. As the parameter value increases, the proportion of reforming products decreases, while the proportion of unreacted methane in the post-reaction mixture increases. As evidenced by the results, the network could correctly reproduce the post-reaction mixture composition for a wide range of steam-to-methane ratios.

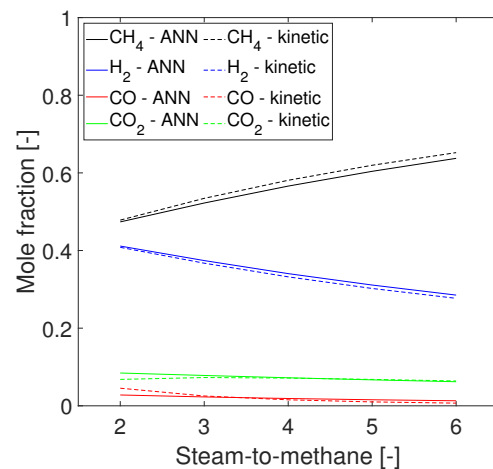


Figure 6. Comparison of ANN simulation results with test data (kinetic simulation data) for variable steam-to-methane ratio values and $T = 700\text{ °C}$; $NC = 1.00$; $f_{CH_4} = 3.38 \cdot 10^{-5}\text{ mol s}^{-1}$; $m_{Ni} = 1.48\text{ g}$.

Figure 7 shows the concentrations of components in the post-reaction mixture as a function of reaction temperature. Experimental results are presented as points, whereas continuous lines represent ANN predictions. It can be observed that with increasing temperature, the methane content decreases, while the hydrogen, carbon monoxide, and carbon dioxide contents increase, indicating an increased methane conversion rate. The discrepancy between the artificial neural network prediction and the experiment is noticeably higher at a higher temperature. This might be due to using a theoretical dataset obtained with a mathematical model that has several important simplifications: (1) It assumes that the steam reforming process consists of two reactions: methane steam reforming and the shift reaction. The use of a simple model neglects other reactions in the process. (2) It assumes that a kinetic equation describes the steam reforming reaction, but the shift reaction occurs close to its equilibrium. This is a widespread assumption, as evidenced by various articles [32,33]; however, it is not necessarily precise under specific conditions [34]. This indicates that the neural network

model could be further improved by including results from both kinetic and equilibrium regimes and theoretical data that can handle both in the dataset.

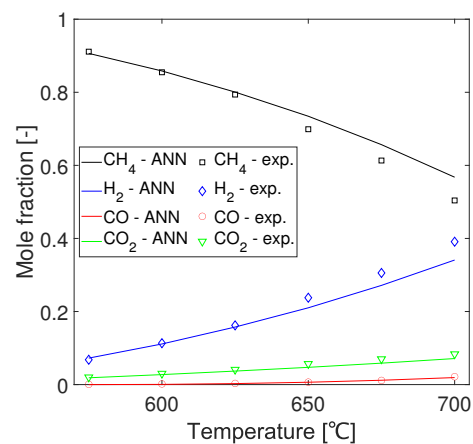


Figure 7. Comparison of ANN simulation results with test data (experimental data) for variable temperature values and $SC = 3.00$; $NC = 3.00$; $f_{CH_4} = 3.38 \cdot 10^{-5} \text{ mol s}^{-1}$; $m_{Ni} = 1.48 \text{ g}$.

When analyzing the trends from Figures 4–7, it is crucial to consider that the data utilized for training were obtained within a kinetic regime, significantly distant from the reaction equilibrium. Most importantly, a good agreement between simulation results and test data is found for those crucial relations. The simulation resulted in a function that is characterized by continuous derivatives, which builds trust in the prediction of the proposed neural network.

Figure 8 presents the comparison of the hydrogen fractions in the post-reaction mixture obtained by the ANN simulation, the experiment, and the kinetic simulation. Experimental data are presented as blue points, and kinetic simulation data as green ones. There is a good agreement between the artificial neural network outcomes and both the experimental and theoretical data. This indicates that the training process proceeded correctly, and the network was able to accurately predict the composition of the post-reaction mixture. It can be observed that the predictions of the network exhibit greater consistency with the results of the kinetic simulation than with the experimental outcomes. The network has become similar to the kinetic model due to the excessive amount of theoretical data utilized, resulting from the limited availability of experimental data. The most significant discrepancy between the experimental data and the ANN prediction results is observed in the range of higher hydrogen fractions. This could be due to the reaction reaching an equilibrium state, which was not accounted for in the mathematical model.

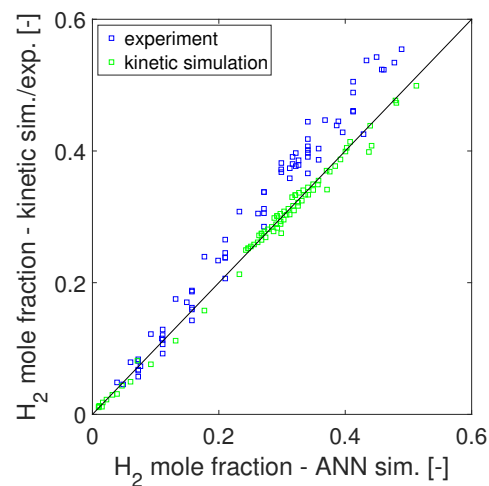


Figure 8. Comparison of ANN simulation results with experiment and kinetic simulation results.

Table 4 presents the comparison of the mean squared error values obtained by four different models of reforming reactions. A two-layer ANN with a sigmoid function and a nonlinear response surface model [17] were used to predict hydrogen yield based on methane partial pressure, steam partial pressure, and the temperature of the reaction. The two-layer ANN achieved a lower error (equal to 0.12) than the nonlinear response surface model (0.23). The mathematical model used in this study yielded an MSE value equal to 0.0032. The designed ANN was characterized by the lowest error value, which was 0.00022.

Table 4. Comparison of mean squared error values for selected methane steam reforming models.

Model	MSE
3-Layer ANN with sigmoid and softmax function	0.00022
Mathematical kinetic model	0.0032
2-Layer ANN with sigmoid function [17]	0.12
Nonlinear response surface model [17]	0.23

Based on the presented results, some limitations of the designed model can be observed. The network excessively conformed to the kinetic model. This is caused by the excessive weight assigned to the theoretical data, which only included the kinetics of the reforming reactions. Two solutions could be implemented to enhance the ANN performance. Firstly, gathering more experimental data would allow for a more accurate consideration of their significance through augmentation. Additionally, incorporating an equilibrium reaction model would improve the simulation prediction in conditions closer to the equilibrium state (for example, at higher temperatures).

4. Conclusions

This paper presents an artificial neural network designed as a model for the methane steam reforming process. The network predicted the composition of the post-reaction mixture based on variable values of the reactor operating parameters. Augmentation techniques were used by including experimental, interpolated, and theoretical data in the training process, with categories of importance assigned to each type of data. The optimal network structure was selected on the basis of statistical analysis, including a mean squared error equal to 0.00022, a Pearson correlation coefficient of 0.97, and a Spearman correlation coefficient of 1.00. ANN predictions were compared with test data to further verify its performance. The outcomes of the simulation demonstrated a strong correlation with the test data across all the incorporated operating parameters. The ANN simulation yielded a function characterized by continuous derivatives. Based on the above, the ANN turned out to be an adequate model of the process under the investigated conditions. An observable constraint to the constructed model is caused by the excessive weight assigned to the theoretical data. The network exhibited an excessive resemblance to the kinetic model. It will be necessary to gather more experimental data and also include equilibrium and more generalized reaction models for theoretical data generation to further enhance the model performance.

Author Contributions: Conceptualization, G.B. (calculations) and S.K. (experiment); methodology, G.B.; software, Z.P.; validation, Z.P. and G.B.; formal analysis, Z.P.; investigation, Z.P.; resources, G.B. and S.K.; data curation, Z.P.; writing—original draft preparation, Z.P.; writing—review and editing, G.B.; visualization, Z.P.; supervision, S.K.; project administration, G.B.; funding acquisition, G.B. All authors have read and agreed to the published version of the manuscript.

Funding: This research was funded by the Polish National Agency for Academic Exchange under the Strategic Partnerships Programme, Project No. BPI/PST/2021/1/00023 (project title: Strategic cooperation with Japan in the field of Energy and Environmental Engineering).

Data Availability Statement: The used dataset is available on reasonable request.

Acknowledgments: The authors would like to express their gratitude to Janusz Szmyd for his invaluable support in fostering the collaboration between AGH and SIT, which made this research possible.

Conflicts of Interest: The authors declare no conflicts of interest. The funders had no role in the design of the study; in the collection, analyses, or interpretation of data; in the writing of the manuscript; or in the decision to publish the results.

Appendix A

Appendix A.1. Comparison of Mean Squared Error Values for Different Network Architectures

Table A1, presented below, shows a comparison of the mean squared error values for the tested network architectures. The mean squared error describes the performance value of the network training process. Variable values of three parameters were tested: the number of hidden layers, the number of neurons in the hidden layers, and the number of epochs. The lowest achieved error value was 0.000199 for the network labeled as number twenty-three. This network consisted seven hidden layers with a configuration of 5-12-14-16-14-12-10-4, and the training process lasted for 4000 epochs.

Table A1. Mean squared error values for subsequent network architecture variants.

No.	Number of Hidden Layers	Vector of the Number of Neurons in Hidden Layers	Number of Epochs	Mean Squared Error
1	2	[2 2]	300	0.000404
2	2	[2 2]	2000	0.000351
4	2	[4 4]	500	0.000412
3	2	[4 4]	1000	0.00029
5	3	[2 4 2]	2000	0.000389
6	3	[2 4 2]	5000	0.000358
7	3	[2 4 2]	10,000	0.000389
8	3	[4 6 4]	5000	0.000386
9	3	[4 6 4]	20,000	0.000386
10	3	[6 8 6]	5000	0.000248
11	3	[6 8 6]	6000	0.000217
12	3	[6 8 6]	10,000	0.000338
13	4	[2 4 6 4]	5000	0.000413
14	4	[2 4 6 4]	7000	0.000398
15	4	[6 8 6 4]	10,000	0.000458
16	4	[6 8 6 4]	25,000	0.000282
17	5	[6 8 10 8 6]	40,000	0.000237
18	5	[6 8 10 8 6]	20,000	0.000319
19	5	[8 10 12 10 8]	5000	0.000346
20	5	[8 10 12 10 8]	25,000	0.000218
21	6	[10 12 14 12 10 8]	10,000	0.000295
22	6	[10 12 14 12 10 8]	20,000	0.000361
23	7	[12 14 16 14 12 10 8]	4000	0.000199
24	7	[12 14 16 14 12 10 8]	36,000	0.000225

References

- Hassan, Q.; Algburi, S.; Sameen, A.Z.; Jaszczur, M.; Salman, H.M. Hydrogen as an energy carrier: Properties, storage methods, challenges, and future implications. *Environ. Syst. Decis.* **2023**. [[CrossRef](#)]
- Hand, E. Hidden hydrogen. *Science* **2023**, *379*, 630–636. [[CrossRef](#)]
- Truche, L.; Donzé, F.V.; Goskolli, E.; Muceku, B.; Loisy, C.; Monnin, C.; Dutoit, H.; Cerepi, A. A deep reservoir for hydrogen drives intense degassing in the Bulqizë ophiolite. *Science* **2024**, *383*, 618–621. [[CrossRef](#)]
- International Energy Agency. Global Hydrogen Review 2023. 2023. Available online: <https://www.iea.org/reports/global-hydrogen-review-2023> (accessed on 10 April 2024).
- Holladay, J.; Hu, J.; King, D. L.; Wang, Y. An overview of hydrogen production technologies. *Catal. Today* **2009**, *139*, 244–260. [[CrossRef](#)]

6. Boretti, A.; Banik, B.K. Advances in Hydrogen Production from Natural Gas Reforming. *Adv. Energy Sustain. Res.* **2021**, *2*, 2100097. [[CrossRef](#)]
7. Fowles, M.; Carlsson, M. Steam Reforming of Hydrocarbons for Synthesis Gas Production. *Top. Catal.* **2021**, *64*, 856–875. [[CrossRef](#)]
8. Ganguli, A.; Bhatt, V. Hydrogen production using advanced reactors by steam methane reforming: A review. *Front. Therm. Eng.* **2023**, *3*, 1143987. [[CrossRef](#)]
9. Baek, S.M.; Kang, J.H.; Lee, K.J.; Nam, J.H. A numerical study of the effectiveness factors of nickel catalyst pellets used in steam methane reforming for residential fuel cell applications. *Int. J. Hydrogen Energy* **2014**, *39*, 9180–9192. [[CrossRef](#)]
10. Wójcik, M.; Szablowski, Ł.; Dybiński, O. Comparison of mathematical models of steam methane reforming process for the needs of fuel cells. *Int. J. Hydrogen Energy* **2024**, *52*, 965–982. [[CrossRef](#)]
11. Brus, G.; Komatsu, Y.; Kimijima, S.; Szmyd, J. An Analysis of Biogas Reforming Process on Ni/YSZ and Ni/SDC Catalysts. *Int. J. Thermodyn.* **2012**, *15*, 43–51.
12. van Biert, L.; Visser, K.; Aravind, P. Intrinsic methane steam reforming kinetics on nickel-ceria solid oxide fuel cell anodes. *J. Power Sources* **2019**, *443*, 227261. [[CrossRef](#)]
13. Chen, K.; Zhao, Y.; Zhang, W.; Feng, D.; Sun, S. The intrinsic kinetics of methane steam reforming over a nickel-based catalyst in a micro fluidized bed reaction system. *Int. J. Hydrogen Energy* **2020**, *45*, 1615–1628. [[CrossRef](#)]
14. Pashchenko, D.; Eremin, A. Heat flow inside a catalyst particle for steam methane reforming: CFD-modeling and analytical solution. *Int. J. Heat Mass Transf.* **2021**, *165*, 120617. [[CrossRef](#)]
15. Amini, A.; Sedaghat, M.H.; Jamshidi, S.; Shariati, A.; Rahimpour, M.R. A comprehensive CFD simulation of an industrial-scale side-fired steam methane reformer to enhance hydrogen production. *Chem. Eng. Process. Process. Intensif.* **2023**, *184*, 109269. [[CrossRef](#)]
16. Vo, N.D.; Oh, D.H.; Hong, S.H.; Oh, M.; Lee, C.H. Combined approach using mathematical modelling and artificial neural network for chemical industries: Steam methane reformer. *Appl. Energy* **2019**, *255*, 113809. [[CrossRef](#)]
17. Ayodele, B.V.; Alsaffar, M.A.; Mustapa, S.I.; Adesina, A.; Kanthasamy, R.; Witoon, T.; Abdullah, S. Process intensification of hydrogen production by catalytic steam methane reforming: Performance analysis of multilayer perceptron-artificial neural networks and nonlinear response surface techniques. *Process. Saf. Environ. Prot.* **2021**, *156*, 315–329. [[CrossRef](#)]
18. Nkulikiyinka, P.; Yan, Y.; Güleç, F.; Manovic, V.; Clough, P.T. Prediction of sorption enhanced steam methane reforming products from machine learning based soft-sensor models. *Energy AI* **2020**, *2*, 100037. [[CrossRef](#)]
19. Liu, Z.; Tian, W.; Cui, Z.; Liu, B. A universal microkinetic-machine learning bimetallic catalyst screening method for steam methane reforming. *Sep. Purif. Technol.* **2023**, *311*, 123270. [[CrossRef](#)]
20. Wang, Y.; Wu, C.; Zhao, S.; Wang, J.; Zu, B.; Han, M.; Du, Q.; Ni, M.; Jiao, K. Coupling deep learning and multi-objective genetic algorithms to achieve high performance and durability of direct internal reforming solid oxide fuel cell. *Appl. Energy* **2022**, *315*, 119046. [[CrossRef](#)]
21. Vo, N.D.; Kang, J.H.; Oh, D.H.; Jung, M.Y.; Chung, K.; Lee, C.H. Sensitivity analysis and artificial neural network-based optimization for low-carbon H₂ production via a sorption-enhanced steam methane reforming (SESMR) process integrated with separation process. *Int. J. Hydrogen Energy* **2022**, *47*, 820–847. [[CrossRef](#)]
22. Mehrabian, M.; Mahmoudimehr, J. A correlation for optimal steam-to-fuel ratio in a biogas-fueled solid oxide fuel cell with internal steam reforming by using Artificial Neural Networks. *Renew. Energy* **2023**, *219*, 119397. [[CrossRef](#)]
23. Hossain, M.A.; Ayodele, B.V.; Cheng, C.K.; Khan, M.R. Artificial neural network modeling of hydrogen-rich syngas production from methane dry reforming over novel Ni/CaFe₂O₄ catalysts. *Solid State Ionics* **2016**, *41*, 11119–11130. [[CrossRef](#)]
24. Deng, H.; Guo, Y. Artificial Neural Network Model for the Prediction of Methane Bi-Reforming Products Using CO₂ and Steam. *Processes* **2022**, *10*, 1052. [[CrossRef](#)]
25. Pajak, M.; Brus, G.; Szmyd, J.S. Genetic algorithm-based strategy for the steam reformer optimization. *Int. J. Hydrogen Energy* **2023**, *48*, 11652–11665. [[CrossRef](#)]
26. Pajak, M.; Brus, G.; Kimijima, S.; Szmyd, J.S. Coaxial multi-criteria optimization of a methane steam reforming reactor for effective hydrogen production and thermal management. *Energy AI* **2023**, *13*, 100264. [[CrossRef](#)]
27. Pajak, M.; Brus, G.; Kimijima, S.; Szmyd, J.S. Enhancing Hydrogen Production from Biogas through Catalyst Rearrangements. *Energies* **2023**, *16*, 4058. [[CrossRef](#)]
28. Morlanés, N.; Lezcano, G.; Yerrayya, A.; Mazumder, J.; Castaño, P. Improving robustness of kinetic models for steam reforming based on artificial neural networks and ab initio calculations. *Chem. Eng. J.* **2022**, *433*, 133201. [[CrossRef](#)]
29. Bilgiç, G.; Bendeş, E.; Öztürk, B.; Atasever, S. Recent advances in artificial neural network research for modeling hydrogen production processes. *Int. J. Hydrogen Energy* **2023**, *48*, 18947–18977. [[CrossRef](#)]
30. Brus, G. Experimental and numerical studies on chemically reacting gas flow in the porous structure of a solid oxide fuel cells internal fuel reformer. *Int. J. Hydrogen Energy* **2012**, *37*, 17225–17234. [[CrossRef](#)]
31. AGC Seimi Chemical Co. Catalyst Analysis Sheets. In *Technical Data Sheets*; AGC Seimi Chemical Co.: Chigasaki, Japan, 2009.
32. Mozdierz, M.; Brus, G.; Kimijima, S.; Szmyd, J.S. Numerical analysis of helium-heated methane/steam reformer. *J. Physics Conf. Ser.* **2016**, *745*, 032081. [[CrossRef](#)]

33. Nishino, T.; Szmyd, J.S. Numerical analysis of a cell-based indirect internal reforming tubular SOFC operating with biogas. *J. Fuel Cell Sci. Technol.* **2010**, *7*, 0510041–0510048. [[CrossRef](#)]
34. Ahmed, K.; Föger, K. Approach to equilibrium of the water-gas shift reaction on a Ni/zirconia anode under solid oxide fuel-cell conditions. *J. Power Sources* **2001**, *103*, 150–153. [[CrossRef](#)]

Disclaimer/Publisher’s Note: The statements, opinions and data contained in all publications are solely those of the individual author(s) and contributor(s) and not of MDPI and/or the editor(s). MDPI and/or the editor(s) disclaim responsibility for any injury to people or property resulting from any ideas, methods, instructions or products referred to in the content.